Check for updates

Original Paper

MEASUREMENT AND CONTROL

Measurement and Control
1–17
© The Author(s) 2020
Article reuse guidelines:
sagepub.com/journals-permissions
DOI: 10.1177/0020294020944961
journals.sagepub.com/home/mac
SAGE

Trajectory planning and tracking control for autonomous parallel parking of a non-holonomic vehicle

Jiaxu Zhang[1,2], Zhengtang Shi[3], Xiong Yang[3] and Jian Zhao[1]

Abstract

This paper proposes autonomous parallel parking for a front-wheel steering vehicle, with highlights on a trajectory planning method and on a trajectory tracking control method. The trajectory planning problem is decoupled into the path planning problem and the longitudinal velocity planning problem to reduce the difficulty of the trajectory planning problem. First, a collision-free path by combining circle arcs with straight line is created to park the vehicle in one or more maneuvers on the premise of meeting the kinematic constraint of vehicle, and then the path is transformed into a continuous-curvature path using B-spline curve. Second, the longitudinal velocity is created using B-spline curve on the premise of meeting the performance constraints of driving and braking system. To execute the generated trajectory, a non-time reference path tracking sliding mode control strategy is deduced by Lyapunov stability theory, and a longitudinal velocity tracking proportional–integral control strategy is proposed based on smooth handoff method. Finally, the parking performance is verified based on model-in-the-loop simulation system.

Keywords

Autonomous parallel parking, trajectory planning, trajectory tracking control, B-spline curve

Date received: 5 February 2020; accepted: 4 June 2020

Introduction

Nowadays, the autonomous driving has become an increasingly significant theme for automotive industry.[1–3] The autonomous parking, which is a solution to solve the problem of "parking difficulty" for the inexperienced or unskilled drivers, is considered as a special topic in the autonomous driving. One major challenge of developing the autonomous parking comes from the fact that it has low computation cost and meets non-holonomic constraints of the vehicle.[4] For the challenge, numerous experts and scholars have been committed to research works of this topic and many different methods have been utilized.

These methods can be divided into two types: methods based on artificial intelligence technology and methods based on planning–tracking framework. Moran and Nagai[5] proposed a novel design method to achieve automatic parallel parking of vehicle using fuzzy-neural network with the vehicle pose and the steering wheel angle for input and output, respectively. Zhao and Collins[6] deduced a robust adaptive algorithm for automatic parallel parking in tight space by combining fuzzy logic system with genetic algorithm, which can tune the parameters of the fuzzy logic system adaptively. Ryu et al.[7] regarded the vehicle pose and the steering angle as input and output of fuzzy logic system, and presented a parallel parking algorithm based on the fuzzy logic system. Lee et al.[8] designed and implemented a novel intelligent control strategy for autonomous vehicle parking by integrating genetic algorithm, Petri net and fuzzy logic system. Demirli and Khoshnejad[9] adopted the sampling points on the fifth-order polynomial reference paths as training data, and then the fuzzy inference-based adaptive network system was trained to imitate the parallel parking operation of skilled drivers. Zheng et al.[10] proposed a new idle ant effect-based algorithm to tune the parameters of the proposed parallel parking fuzzy controller for improving the stability and response speed of the system. Wang and Zhu[11] proposed a hybrid fuzzy

[1]State Key Laboratory of Automotive Simulation and Control, Jilin University, Changchun, China
[2]Intelligent Network R&D Institute, China FAW Group Co., Ltd., Changchun, China
[3]Intelligent Vehicle Control System Research Institute, Zhejiang Asia-Pacific Mechanical and Electronic Co., Ltd., Hangzhou, China

Corresponding author:
Jian Zhao, State Key Laboratory of Automotive Simulation and Control, Jilin University, Changchun 130022, China.
Email: zhaojian@jlu.edu.cn

Creative Commons CC BY: This article is distributed under the terms of the Creative Commons Attribution 4.0 License (https://creativecommons.org/licenses/by/4.0/) which permits any use, reproduction and distribution of the work without further permission provided the original work is attributed as specified on the SAGE and Open Access pages (https://us.sagepub.com/en-us/nam/open-access-at-sage).

autonomous parking system by combining a supervisory fuzzy controller with a base fuzzy controller. The supervisory fuzzy was used to plan an executable parking trajectory, and the base fuzzy controller was designed to track the trajectory by controlling the steering wheel angle and vehicle speed. Liu et al.[12] adopted a deep neural network with the speed and the target pose of vehicle for the input and the vehicle control instructions for the output to establish the nonlinear relationship between the planned parking trajectories and the vehicle control instructions to achieve autonomous parallel parking. Xu et al.[13] presented an automatic parking control strategy by combining sliding mode control method with fuzzy logical control method to expand the initial feasible region. The sliding mode control method was used to guide the vehicle from the initial pose to the intermediate pose, and the fuzzy logical control method was used to drive the vehicle from the intermediate pose to the target pose. These methods based on artificial intelligence technology can effectively solve the problem of "parking difficulty" in the fixed scenes, and usually rely on a larger number of experimental data and expert knowledge to adapt to the changes of parking environment and parking space. However, the acquisition of experimental data and expert knowledge usually requires a large amount of experimental resources and human costs.

Compared with the methods based on artificial intelligence technology, the methods based on planning–tracking framework depend on a fewer number of experimental data and expert knowledge to adapt to the changes of parking environment and parking space. Xu et al.[14] divided the parallel parking environment into the lightly constrained zone and the highly constrained zone, and correspondingly divided the vehicle state into the initial state, the intermediate state and the target state. The path between the initial state and the intermediate state was planned based on realized by combination of circle arcs and straight line, while the path between the intermediate state and the target state is realized by quintic polynomial curves. Zhdanov et al.[15] planned a single-step parallel parking path by combination of circle arcs and straight line, but it is difficult to track the planned path smoothly because of the discontinuous curvature of the planned path. Kim et al.[16] planned a cluster of parking paths using traditional back propagation algorithm, and the cost of each path was calculated in terms of safety and the traveled distance. Finally, the path with the lowest cost was selected as the reference parking path. Zhao et al.[17] planned the collision-free smooth trajectory based on Bezier curve for the autonomous parking system on the premise of meeting the kinematic constraints of the vehicle, and designed a fuzzy proportional–integral–derivative (PID) controller to track the planned trajectory. Chand et al.[18] proposed a new automatic parallel parking maneuver for intelligent vehicles based on the sigmoidal Gompertz curve with four tunable parameters, which were determined by using an optimization scheme. Vorobieva et al.[19] presented a continuous-curvature path-planning method based on circle arcs and clothoid curves, and then the desired steering wheel angle and vehicle speed were calculated to execute the planned path. Jang et al.[20] considered the trajectory planning problem as the constrained optimization problem comprised of vehicle dynamics model and the constraint of the drivable region, and then interior point method was used to solve the optimization problem to generate the feasible parallel parking trajectory. Zips et al.[21] proposed a fast optimization-based path planner for vehicle parking in narrow environments, and the proposed approach could adapt to different parking scenarios by adjusting the weight terms of the cost function of the optimization problem. Chai et al.[22] presented a multilayer optimization strategy for generating the optimal trajectory of autonomous parallel parking system, and the optimization problem was solved by improved particle swarm optimization algorithm and gradient-based algorithm. Yang et al.[23] presented a smooth path-planning algorithm for autonomous parking system by connecting circle arcs, straight line and linearly steering spiral, and then a closed-loop controller was designed to guide the vehicle to follow the planned path. These methods based on planning–tracking framework have the characteristic of global optimization, and can safely drive the vehicle into the target parking space on the premise of meeting the kinematic and dynamic constraints of the vehicle and parking performance indicators.

In this paper, a novel trajectory planning and tracking control method for autonomous parallel parking of a front-wheel steering vehicle is presented. For the sake of reducing the difficulty of the trajectory planning problem, it is decoupled into the path planning problem and the longitudinal velocity planning problem by choosing the arc length of the trajectory as the path velocity correlation term. That is, the planning problem in three-dimensional space is simplified to two planning problems in two-dimensional space. Considering the kinematic constraint of vehicle, a collision-free path by combining circle arcs with straight line is created to park the vehicle in one or more maneuvers if the parking space is very narrow, and then the path is transformed into a continuous-curvature path using B-spline curve. Moreover, the longitudinal velocity is created using B-spline curve on the premise of meeting the performance constraints of the driving and braking system. To execute the generated trajectory, a non-time reference path tracking sliding mode control strategy is deduced by Lyapunov stability theory, and a longitudinal velocity tracking PI control strategy is proposed based on smooth handoff method. Finally, the parking performance is verified based on model-in-the-loop simulation system.

The rest of this paper is structured as follows. Section "Trajectory planning" gives the collision-free smooth trajectory for guiding the vehicle to enter the

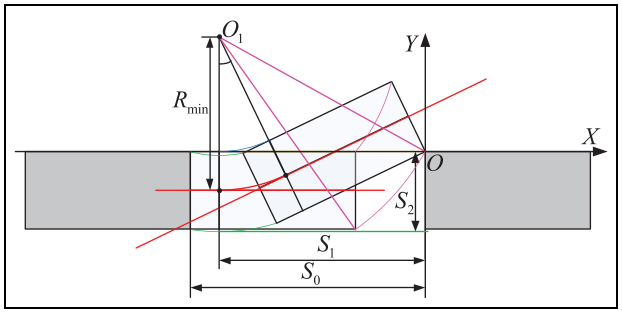

Figure 1. Minimal length and width of the parking space for parking in one maneuver.

parking space in one or more maneuvers based on the combination of circle arcs, straight line, and B-spline curves. Section "Trajectory tracking control" deduces and analyses the non-time reference path tracking sliding mode control strategy and the longitudinal velocity tracking PI control strategy. Section "Simulation results" validates the parking performance, and section "Conclusion" gives the main conclusion of our work.

Trajectory planning

Trajectory planning is to design a collision-free and practical trajectory, which could guide the vehicle to the parking space safely, accurately and quickly. In this section, the trajectory planning problem for autonomous parallel parking of a front-wheel steering vehicle is decoupled into the path planning problem and the longitudinal velocity planning problem by choosing the arc length of the trajectory as the path velocity correlation term. Specifically, a collision-free path by combining circle arcs with straight line is created to park the vehicle in one or more maneuvers on the premise of meeting the kinematic constraint of vehicle, and then the path is transformed into a continuous-curvature path based on B-spline curve. Moreover, the longitudinal velocity is created based on B-spline curve on the premise of meeting the performance constraints of driving and braking system.

One-maneuver path planning

The vehicle is running at low speed when parking, so it is assumed to move with the four wheels rolling without slipping around the same instantaneous center. As shown in Figure 1, we take the left front corner of the parking space as the origin of the global coordinate system OXY and define the midpoint of the vehicle's rear wheel axle as the reference point of the vehicle. The feasibility problem of parking in one maneuver can be solved in the reverse way by retrieving the vehicle from the parking space. The minimum length of the parking space for parking in one maneuver is deduced by making the right front corner of the vehicle having no collision with the front obstacle when the vehicle rotates with the minimum radius $R_{\min}$ to exit the parking space

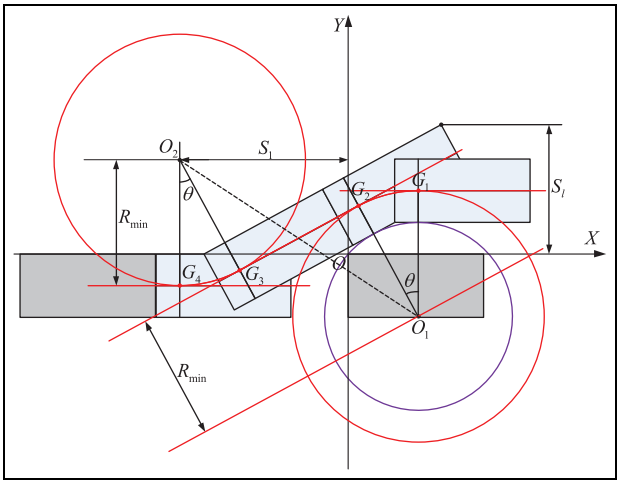

Figure 2. Path for parking in one maneuver.

$$S_0 = S_1 + L_r = \sqrt{(L + L_f)^2 + \left(R_{\min} + \frac{W}{2}\right)^2 - \left(R_{\min} - \frac{W}{2}\right)^2} + L_r = \sqrt{(L + L_f)^2 + 2R_{\min}W} + L_r \quad (1)$$

where L is the wheelbase; W is the width of the vehicle; L_f and L_r are the front and rear overhangs, respectively.

Similarly, the minimum width of the parking space for parking in one maneuver is deduced by making the right rear corner of the vehicle have no collision with the lateral obstacle when the vehicle rotates with the minimum radius $R_{\min}$ to exit the parking space

$$S_2 = \sqrt{\left(R_{\min} + \frac{W}{2}\right)^2 + L_r^2} - \left(R_{\min} - \frac{W}{2}\right) \quad (2)$$

Supposing that the length and width of the parking space is larger than the minimum length and width of the parking space for parking in one maneuver, the task of one-maneuver path planning is to generate a collision-free path based on the combination of circle arcs and straight line under the conditions that the coordinate of the starting point G_1 is known as (x_{G_1}, y_{G_1}) and the coordinate of the target point G_4 is known as $(-S_1, -W/2)$. As shown in Figure 2, the specific process of one-maneuver path planning is as follows:

1. According to the coordinate of the starting point G_1, the coordinate of the center point O_1 of the circle arc G_5G_6 is calculated as $(x_{G_1}, y_{G_1} - R_{\min})$.
2. According to the coordinate of the target point G_4, the coordinate of the center point O_2 of the

circle arc $\overset{\frown}{G_1G_2}$ is calculated as $(-S_1, R_{\min} - W/2)$.

3. The angle of circle arc $\overset{\frown}{G_1G_2}$ and circle arc $\overset{\frown}{G_3G_4}$ are given by

$$\theta = \arcsin\left(\frac{x_{G_1} + S_1}{|O_1O_2|}\right) - \arccos\left(\frac{2R_{\min}}{|O_1O_2|}\right) \tag{3}$$

4. The coordinate of the point G_2 is calculated as $(x_{G_1} - R_{\min}\sin\theta, y_{G_1} - R_{\min}(1-\cos\theta))$, and the coordinate of the point G_3 is calculated as $(-S_1 + R_{\min}\sin\theta, R_{\min}(2-\cos\theta) - W/2)$.
5. The maximum distance from the x-axis of the coordinate system OXY to the envelope of the planned path is calculated as

$$S_l = \left(R_{\min} + \frac{W}{2}\right)\cos(\min(\theta, \vartheta_{\max})) + \left(L + L_f\right)\sin(\min(\theta, \vartheta_{\max})) + y_{G_1} - R_{\min} \tag{4}$$

where $\vartheta_{\max} = \arctan\left((L + L_f)/(R_{\min} + W/2)\right)$.

According to equation (3), the angle of circle arc $\overset{\frown}{G_1G_2}$ and circle arc $\overset{\frown}{G_3G_4}$ increases with the decrease of the x coordinate of the starting point G_1 when the y coordinate of the starting point G_1 remains constant. According to equation (4), the maximum distance S_l increases with the increase of the angle of circle arc $\overset{\frown}{G_1G_2}$ and circle arc $\overset{\frown}{G_3G_4}$ when $\theta \leqslant \vartheta_{\max}$. Therefore, the maximum distance S_l increases with the decrease of the x coordinate of the starting point G_1 when $\theta \leqslant \vartheta_{\max}$.

Multiple maneuvers path planning

When the length of the parking space is smaller than the minimum length of the parking space for parking in one maneuver, the vehicle first moves backward along one maneuver path until approaching the rear obstacle, and then moves forward with the maximum steering wheel angle to parallel to the parking space and approach the front obstacle. Subsequently, a series of forward and backward moves is designed to make the vehicle enter into the parking space, as shown in Figures 3–6.

Forward move. Supposing that the available longitudinal distance m_1 is sufficient, the goal of the forward move is to maximize the lateral displacement on the premise that the vehicle is parallel to the parking space at the end of forward move. As shown in Figure 3, the vehicle moves along the circle arc $\overset{\frown}{G_1G_2}$ with the radius R to approach the lateral obstacle. According to the relationship among the fixed coordinate system G_1XY, the translational coordinate system G_2XY and the body coordinate system G_2xy, the equation of motion of the right front corner of the vehicle in the vector-matrix form is given by

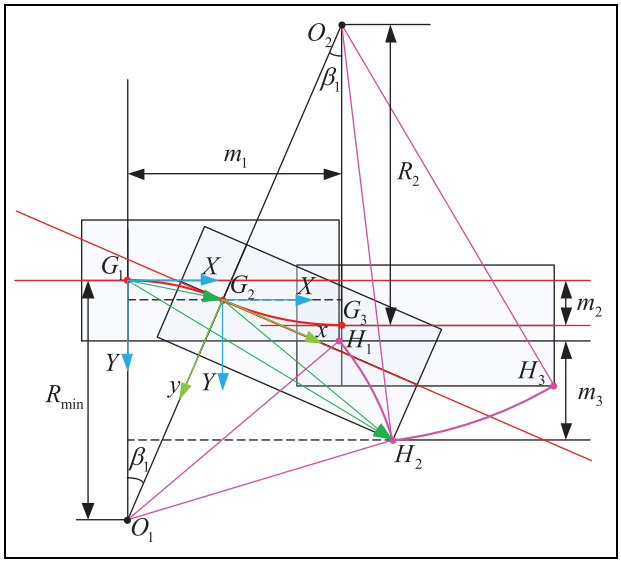

Figure 3. Forward move with sufficient longitudinal distance available.

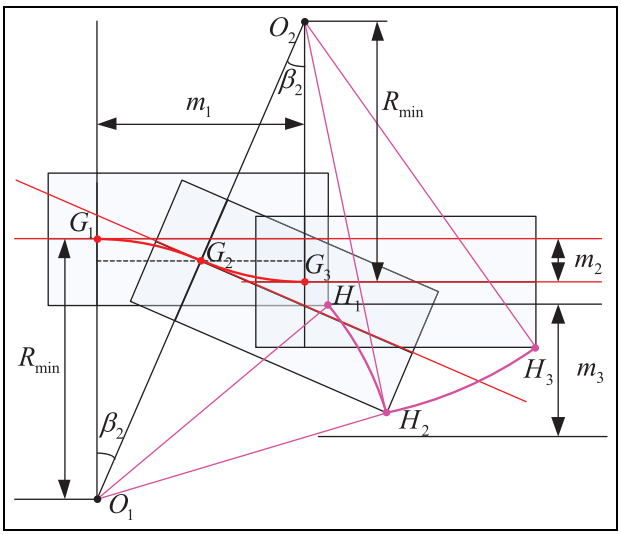

Figure 4. Forward move with sufficient lateral distance available.

$$\overrightarrow{G_1H_2} = \overrightarrow{G_1G_2} + \overrightarrow{G_2H_2} = \begin{bmatrix} R\sin\beta \\ R(1-\cos\beta) \end{bmatrix} + \begin{bmatrix} \cos\beta & -\sin\beta \\ \sin\beta & \cos\beta \end{bmatrix}\begin{bmatrix} L + L_f \\ \frac{W}{2} \end{bmatrix} \tag{5}$$

where β is the angle of the circle arc $\overset{\frown}{G_1G_2}$.

The y coordinate of the point H_2 is $m_3 + W/2$, and m_3 is the available lateral distance. According to equation (5), we can obtain

$$R(1-\cos\beta) + \left(L + L_f\right)\sin\beta + \left(\frac{W}{2}\right)\cos\beta = m_3 + \frac{W}{2} \tag{6}$$

According to equation (6), we can obtain

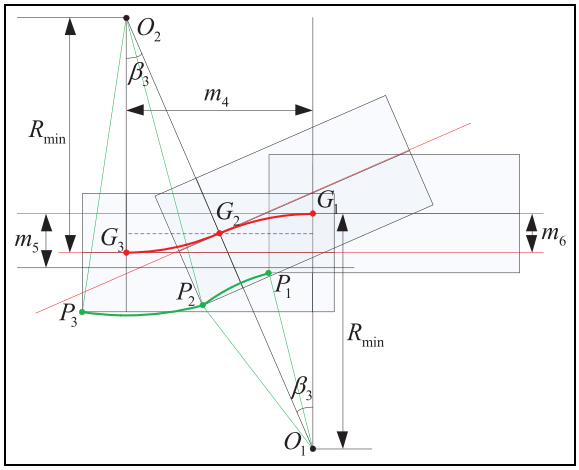

Figure 5. Backward move with sufficient lateral distance available.

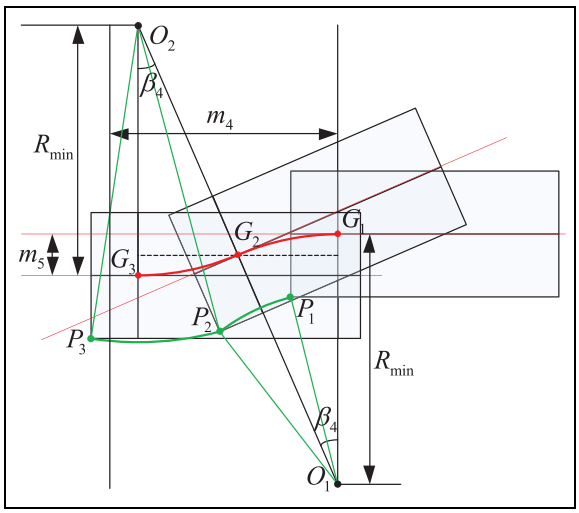

Figure 6. Backward move with sufficient longitudinal distance available.

$$\frac{(R - W/2)\cos\beta - (L + L_f)\sin\beta}{\sqrt{(R - W/2)^2 + (L + L_f)^2}} = \frac{R - m_3 - W/2}{\sqrt{(R - W/2)^2 + (L + L_f)^2}} \tag{7}$$

According to equation (7), when the radius R of the circle arc $\overset{\frown}{G_1G_2}$ is set to the minimum radius $R_{\min}$, the angle of the circle arc $\overset{\frown}{G_1G_2}$ reaches the maximum value described as follows

$$\beta_1 = \arccos\left(\frac{R_{\min} - m_3 - W/2}{\sqrt{(R_{\min} - W/2)^2 + (L + L_f)^2}}\right) - \arctan\left(\frac{L + L_f}{R_{\min} - W/2}\right) \tag{8}$$

Considering the constraint of the available longitudinal distance m_1 and the constraint that the vehicle should be parallel to the parking space at the end of forward move, we can obtain the following equation based on the circle arc $\overset{\frown}{G_1G_2}$ with the radius $R_{\min}$ and the angle β_1

$$m_1 = R_{\min}\sin\beta_1 + R_2\sin\beta_1 \tag{9}$$

where R_2 is the radius of the circle arc $\overset{\frown}{G_2G_3}$, and according to equation (9), we can obtain

$$R_2 = \frac{m_1}{\sin\beta_1} - R_{\min} \tag{10}$$

According to the circle arc $\overset{\frown}{G_1G_2}$ with the radius $R_{\min}$ and the angle β_1 and the circle arc $\overset{\frown}{G_2G_3}$ with the radius R_2 and the angle β_1, the available longitudinal distance m_1 and the lateral displacement m_2 are given by

$$m_1 = (R_{\min} + R_2)\sin\beta_1 \tag{11}$$

$$m_2 = (R_{\min} + R_2)(1 - \cos\beta_1) \tag{12}$$

According to equations (11) and (12), we can obtain

$$\frac{m_2}{m_1} = \frac{1 - \cos\beta_1}{\sin\beta_1} = \tan\frac{\beta_1}{2} \tag{13}$$

Equation (13) shows that the lateral displacement of the vehicle increases with the angle of the circle arc $\overset{\frown}{G_1G_2}$ increased, which is the reason why the minimum radius is adopted as the radius of the circle arc $\overset{\frown}{G_1G_2}$. Furthermore, equation (12) shows that the lateral displacement of the vehicle increases with the radius of the circle arc $\overset{\frown}{G_2G_3}$ increased, which is the reason why the available longitudinal distance m_1 is fully utilized in the calculation of the radius of the circle arc $\overset{\frown}{G_2G_3}$.

Supposing that the available lateral distance m_3 is sufficient, the goal of the forward move is to maximize the lateral displacement on the premise that the vehicle is parallel to the parking space at the end of forward move. As shown in Figure 4, the radii of the circle arc $\overset{\frown}{G_1G_2}$ and the circle arc $\overset{\frown}{G_2G_3}$ are set to the minimum radius $R_{\min}$, we can obtain the following equation based on the constraint of the available longitudinal distance m_1 and the constraint that the vehicle should be parallel to the parking space at the end of forward move

$$m_1 = 2R_{\min}\sin\beta_2 \tag{14}$$

According to equation (14), the angle of the circle arc $\overset{\frown}{G_1G_2}$ and the circle arc $\overset{\frown}{G_2G_3}$ are given by

$$\beta_2 = \arcsin\left(\frac{m_1}{2R_{\min}}\right) \tag{15}$$

Similarly, the lateral displacement of the vehicle is given by

$$m_2 = 2R_{\min}(1 - \cos\beta_2) \tag{16}$$

According to equations (14) and (16), we can obtain

$$\frac{m_2}{m_1} = \frac{1-\cos\beta_2}{\sin\beta_2} = \tan\frac{\beta_2}{2} \tag{17}$$

Equation (17) shows that the lateral displacement of the vehicle increases with the angle of the circle arc $\overset{\frown}{G_1G_2}$ and the circle arc $\overset{\frown}{G_2G_3}$ increased, which is the reason why the minimum radius $R_{\min}$ is used as the radii of the circle arc $\overset{\frown}{G_1G_2}$ and the circle arc $\overset{\frown}{G_2G_3}$.

The above process of designing the forward move of the vehicle is based on the assumptions that the available longitudinal distance of the parking space is sufficient and the available lateral distance of the parking space is sufficient, and the establishing conditions of the assumptions are given by

1. If $\beta_2 > \beta_1$, the available longitudinal distance of the parking space is sufficient, and the forward move of the vehicle is designed based on Figure 3.
2. If $\beta_2 \leqslant \beta_1$, the available lateral distance of the parking space is sufficient, and the forward move of the vehicle is designed based on Figure 4.

Backward move. Supposing that the available lateral distance m_5 is sufficient, the goal of the forward move is to maximize the lateral displacement on the premise that the vehicle is parallel to the parking space at the end of forward move. As shown in Figure 4, the radii of the circle arc $\overset{\frown}{G_1G_2}$ and the circle arc $\overset{\frown}{G_2G_3}$ are set to the minimum radius $R_{\min}$, we can obtain the following equation based on the constraint of the available longitudinal distance m_4 and the constraint that the vehicle should be parallel to the parking space at the end of forward move

$$m_4 = 2R_{\min}\sin\beta_3 \tag{18}$$

According to equation (18), the angle of the circle arc $\overset{\frown}{G_1G_2}$ and the circle arc $\overset{\frown}{G_2G_3}$ are given by

$$\beta_3 = \arcsin\left(\frac{m_4}{2R_{\min}}\right) \tag{19}$$

Similarly, the lateral displacement of the vehicle is given by

$$m_6 = 2R_{\min}(1-\cos\beta_3) \tag{20}$$

According to equations (18) and (20), we can obtain

$$\frac{m_6}{m_4} = \frac{1-\cos\beta_3}{\sin\beta_3} = \tan\frac{\beta_3}{2} \tag{21}$$

Equation (21) shows that the lateral displacement of the vehicle increases with the angle of the circle arc $\overset{\frown}{G_1G_2}$ and the circle arc $\overset{\frown}{G_2G_3}$ increased, which is the reason why the minimum radius $R_{\min}$ is used as the radii of the circle arc $\overset{\frown}{G_1G_2}$ and the circle arc $\overset{\frown}{G_2G_3}$.

Supposing that the available longitudinal distance m_4 is sufficient, the goal of the forward move is to maximize the lateral displacement on the premise that the vehicle is parallel to the parking space at the end of forward move. As shown in Figure 4, the radii of the circle arc $\overset{\frown}{G_1G_2}$ and the circle arc $\overset{\frown}{G_2G_3}$ are set to the minimum radius $R_{\min}$, we can obtain the following equation based on the constraint of the available longitudinal distance m_5 and the constraint that the vehicle should be parallel to the parking space at the end of forward move

$$m_5 = 2R_{\min}(1-\cos\beta_4) \tag{22}$$

According to equation (22), the angle of the circle arc $\overset{\frown}{G_1G_2}$ and the circle arc $\overset{\frown}{G_2G_3}$ are given by

$$\beta_4 = \arccos\left(\frac{2R_{\min}-m_5}{2R_{\min}}\right) \tag{23}$$

After the backward move, the vehicle successfully enters into the parking space.

The above process of designing the backward move of the vehicle is based on the assumptions that the available longitudinal distance of the parking space is sufficient and the available lateral distance of the parking space is sufficient, and the establishing conditions of the assumptions are given by

1. If $\beta_3 < \beta_4$, the available lateral distance of the parking space is sufficient, and the forward move of the vehicle is designed based on Figure 5.
2. If $\beta_3 \geqslant \beta_4$, the available longitudinal distance of the parking space is sufficient, and the forward move of the vehicle is designed based on Figure 6.

Continuous-curvature path for the parking maneuver

The curvature of the parking path by combination of circle arcs and straight line is discontinuous at the junction of circle arc and straight line, and the vehicle has to stop to reorient the steering wheel angle. The steering at the stop induces the non-uniform wear of the tires and increases the workload of the steering motor. Therefore, we adopts B-spline curve to smooth the parking path composed of circle arcs and straight line.

As shown in Figure 7, the curvature of the circle arc $\overset{\frown}{IKK'I'}$ is $1/R_{\min}$, $\angle IOI' = \alpha_1$, $\angle IOK = \alpha_2$, $\angle I'OK' = \alpha_2$. The B-spline curve is used to design the transition curve between the point H and the point K, the curvature of which is continuously and smoothly increased from zero to $1/R_{\min}$, and the angle between the tangent of the circle arc $\overset{\frown}{IKK'I'}$ at the point K and the straight line HO_2 is α_2. Symmetrically, the B-spline curve is used to design the transition curve between the point K' and the point H', the curvature of which is continuously and smoothly reduced from $1/R_{\min}$ to zero, and the

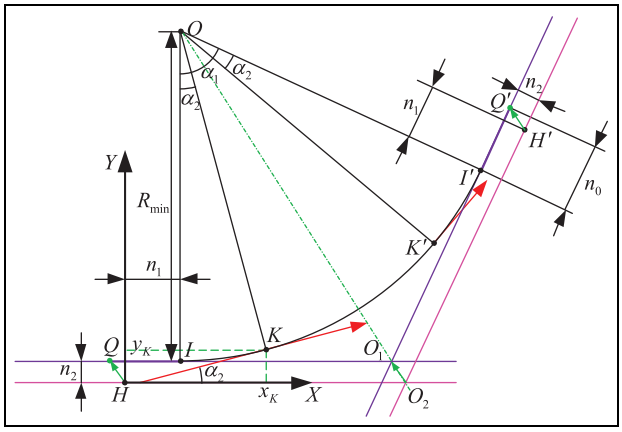

Figure 7. The principle of the parking path smoothed by B-spline curve.

angle between the tangent of the circle arc $\overset{\frown}{IKK'I'}$ at the point K' and the straight line $H'O_2$ is α_2. After smoothing based on the B-spline curve, the triangle $\Delta HO_2H'$ moves in the direction of the vector $\overrightarrow{O_2O_1}$ to make the triangle $\Delta HO_2H'$ and the triangle $\Delta QO_1Q'$ coincided, and the length of the line segment QI or the line segment $I'Q'$ is the length increment of the parking space. Therefore, the B-spline curve is used to complete the smooth transition between circle arc and straight line at the expense of increasing the length of the parking space. As shown in Figure 7, the coordinate system HXY is established, the known coordinate of the point K is (x_K, y_K), the known angle between the tangent of the circle arc $\overset{\frown}{IKK'I'}$ at the point K and the straight line HO_2 is α_2 and the known angle of the circle arc $\overset{\frown}{IKK'I'}$ is α_1. Then, the x coordinate and y coordinate of the point I are given by

$$n_1 = x_K - R_{\min}\sin\alpha_2 \tag{24}$$

$$n_2 = y_K - R_{\min}(1-\cos\alpha_2) \tag{25}$$

According to equations (24) and (25), we can obtain the length of the line segment QI and the line segment $I'Q'$, also known as the smooth offset

$$n_0 = |QI| = |I'Q'| = n_1 + n_2\tan\left(\frac{\alpha_1}{2}\right) \tag{26}$$

According to the definition of B-spline curve,[24] the transition curve based on B-spline curve can be expressed as $C(u) = [x(u), y(u)]^{\mathrm{T}}$. Then, the curvature of the transition curve can be described as

$$\rho = \frac{|\dot{x}\ddot{y} - \ddot{x}\dot{y}|}{\left(\dot{x}^2 + \dot{y}^2\right)^{3/2}} \tag{27}$$

According to the vehicle kinematic model, we can obtain the relationship between the curvature of the transition curve and the front-wheel equivalent steering angle

$$\begin{cases} \tan\delta_f = \frac{L}{R} \\ \rho = \frac{1}{R} \end{cases} \tag{28}$$

Substituting equation (27) into equation (28) yields

$$\delta_f = \arctan\left(\frac{L(\dot{x}\ddot{y} - \ddot{x}\dot{y})}{\left(\dot{x}^2 + \dot{y}^2\right)^{3/2}}\right) \tag{29}$$

According to chain rule, we can obtain the front-wheel equivalent steering speed

$$\varpi = \frac{d\delta_f}{dt} = \frac{d\delta_f}{du}\frac{du}{ds}\frac{ds}{dt} \tag{30}$$

where $du/ds = 1/\sqrt{\dot{x}^2 + \dot{y}^2}$ is the reciprocal of the derivative of the arc length of the parking path with respect to the parameter u; $v = ds/dt$ is the vehicle longitudinal velocity.

Substituting the derivative of equation (29) with respect to the parameter u into equation (30) yields

$$\varpi = \frac{vL\left((\dot{x}\cdot\dddot{y} - \dddot{x}\cdot\dot{y})\left(\dot{x}^2 + \dot{y}^2\right) - 3(\dot{x}\ddot{y} - \ddot{x}\dot{y})(\dot{x}\ddot{x} + \dot{y}\ddot{y})\right)}{\left(\dot{x}^2 + \dot{y}^2\right)^3 + L^2(\dot{x}\ddot{y} - \ddot{x}\dot{y})^2} \tag{31}$$

It is evident from equation (31) that the front-wheel equivalent steering speed is not only related to the parking path, but also related to the vehicle longitudinal velocity. To decouple the parking trajectory planning problem into a path-planning problem and a longitudinal velocity planning problem, equation (31) is rewritten as

$$\varpi = \frac{v_{\max}L\left((\dot{x}\cdot\dddot{y} - \dddot{x}\cdot\dot{y})\left(\dot{x}^2 + \dot{y}^2\right) - 3(\dot{x}\ddot{y} - \ddot{x}\dot{y})(\dot{x}\ddot{x} + \dot{y}\ddot{y})\right)}{\left(\dot{x}^2 + \dot{y}^2\right)^3 + L^2(\dot{x}\ddot{y} - \ddot{x}\dot{y})^2} \tag{32}$$

where $v_{\max}$ is the maximum vehicle longitudinal velocity during the parking process.

According to equations (27) and (32), it can be seen that the continuity of the parking path curvature requires that B-spline curve is C^2 continuous, and the continuity of the front-wheel equivalent steering speed requires that B-spline curve is C^3 continuous. Meanwhile, the inertial effect of the steering motor requires that the front-wheel equivalent steering speed can be continuously changed from zero. Therefore, B-spline curve of degree 5 is selected to design the transition curve. To make B-spline curve pass through the first and last control points, the multiplicities of the first knot and the last knot are set to 6. Thus, the knot vector of the B-spline curve is given by

$$U = \{0,0,0,0,0,0,0.5,1,1,1,1,1,1\} \tag{33}$$

The control points of B-spline curve shown in Figure 8, which are symmetrically distributed on two equal sides of an isosceles triangle, are given by

$$\begin{aligned} P_x = [&0, d\lambda_1, d\lambda_2, d, d(1-(1-\lambda_2)\cos(\phi)), \\ &d(1-(1-\lambda_1)\cos(\phi)), d(1-\cos(\phi))] \end{aligned} \tag{34}$$

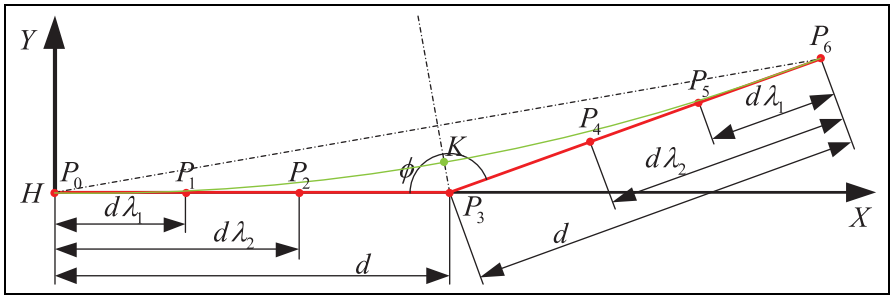

Figure 8. Schematic diagram of B-spline curve of degree five.

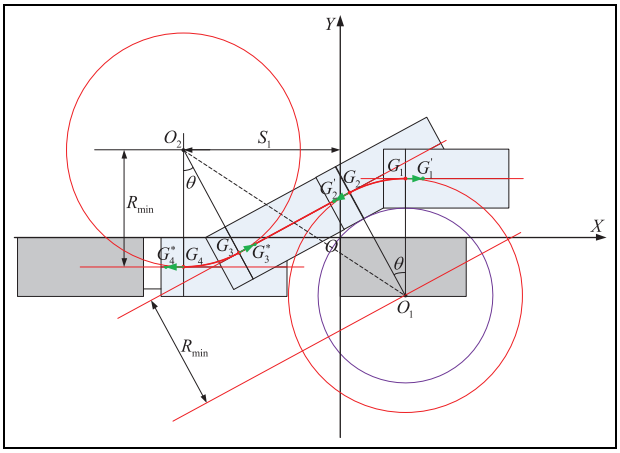

Figure 9. One-maneuver parking path smoothed by B-spline curve.

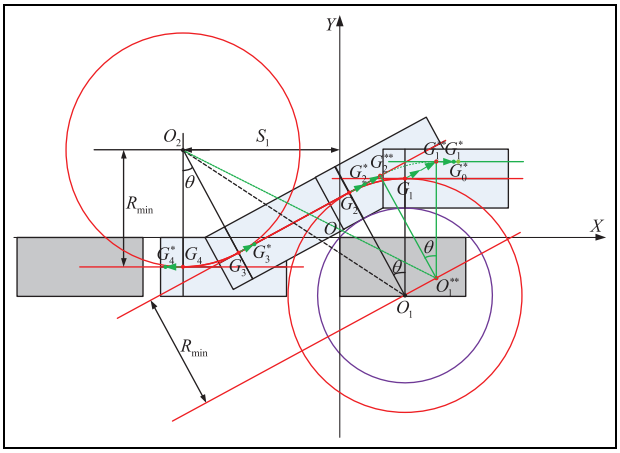

Figure 10. One-maneuver smooth parking path corrected to avoid overlapping path.

$$P_y = [0, 0, 0, 0, d(1-\lambda_2)\sin(\phi), d(1-\lambda_1)\sin(\phi), d\sin(\phi)] \tag{35}$$

where $d>0$, $\pi/2<\phi<\pi$ and $0<\lambda_1<\lambda_2<1$ are unknown parameters.

As shown in Figure 8, the B-spline curve determined by equations (33)–(35) is symmetrical and has the largest curvature at the middle point K of the B-spline curve. Meanwhile, the angle between the tangent of B-spline curve at the point K and x-axis of the coordinate system is $(\pi-\phi)/2$. To minimize the impact of the parking path smoothed by B-spline curve on the length of the parking space, the smooth offset $n_0 = n_1 + n_2\tan(\alpha_1/2) \approx n_1$ should be minimized by adjusting unknown parameters $d>0$, $\pi/2<\phi<\pi$ and $0<\lambda_1<\lambda_2<1$. Therefore, the nonlinear optimization problem (36) is obtained with two constraints. First, the curvature of B-spline curve at the point K should be equal to $1/R_{\min}$. Second, the front-wheel equivalent steering speed should not be greater than the maximum value determined by the performance of the steering motor

$$\begin{aligned} \min_{[d,\phi,\lambda_1,\lambda_2]} \quad & \left(x(0.5) - R_{\min}\sin\left(\frac{\pi-\phi}{2}\right)\right) \\ \text{subject to} \quad & \rho(0.5) = \frac{1}{R_{\min}} \\ & |\varpi| \leqslant \varpi_{\max} \end{aligned} \tag{36}$$

The interior point method[25] is used to solve the nonlinear optimization problem (36) in off-line mode to reduce the computational time, and the first half of the fixed B-spline curve is used as the transition curve.

The parking path composed of circle arcs and straight line shown in Figure 2 is corrected based on the above principle of the parking path smoothed by B-spline curve. As shown in Figure 9, the endpoint G_1 of the circle arc G_1G_2 is corrected to the point G_1', and the coordinate of the point G_1' is $(x_{G_1}+n_0, y_{G_1})$. The endpoint G_2 of the circle arc G_2G_3 is corrected to the point G_2', the coordinate of the point G_2' is $(x_{G_1} - R_{\min}\sin\theta - n_0\cos\theta,\ y_{G_1} - R_{\min}(1-\cos\theta) - n_0\sin\theta)$. The endpoint G_3 of the circle arc G_3G_4 is corrected to the point G_3^*, and the coordinate of the point G_3^* is $(-S_1 + R_{\min}\sin\theta + n_0\cos\theta, R_{\min}(2-\cos\theta) - W/2 + n_0\sin\theta)$. The endpoint G_4 of the circle arc G_3G_4 is corrected to the point G_4^*, and the coordinate of the point G_4^* is $(-S_1 - n_0, -W/2)$.

As shown in Figure 9, the vector $\overrightarrow{G_2G_2'}$ coincides fully or partly with the vector $\overrightarrow{G_3G_3'}$ when the distance between the point G_2 and the point G_3 is less than $2n_0$. As shown in Figure 10, to avoid the coincidence phenomenon, the point G_1' is corrected to the point G_1^*, and the point G_2' is corrected to the point G_2^*. Correspondingly, the circle arc G_1G_2 with the center of the point O_1 is corrected to the circle arc $G_1^{**}G_2^{**}$ with the center of the point O_1^{**}. The coordinate of the point G_1^* is $(x_{G_1} + n_0(1+2\cos\theta), y_{G_1} + 2n_0\sin\theta)$. The

coordinate of the point G_2^* is $(x_{G_1} - R_{\min}\sin\theta + n_0\cos\theta,\ y_{G_1} - R_{\min}(1-\cos\theta) + n_0\sin\theta)$. The coordinate of the point O_1^{**} is $(x_{G_1} + 2n_0\cos\theta,\ y_{G_1} - R_{\min} + 2n_0\sin\theta)$. The coordinate of the point G_1^{**} is $(x_{G_1} + 2n_0\cos\theta, y_{G_1} + 2n_0\sin\theta)$. The coordinate of the point G_2^{**} is $(x_{G_1} - R_{\min}\sin\theta + 2n_0\cos\theta,\ y_{G_1} - R_{\min}(1-\cos\theta) + 2n_0\sin\theta)$. Thus, we can obtain the continuous-curvature parking path $G_1^*G_2^*G_3^*G_4^*$.

The specific smoothing process of the parking path is the inverse process of the above analysis process under the condition that the smoothing offset is unknown. Since the smoothing offset is unknown, a known starting point G_0^* shown in Figure 10 is added to the smoothing process of the parking path. The coordinate of the starting point G_0^* is known as $(x_{G_0^*}, y_{G_0^*})$, and the maximum smoothing offset is known as $n_{\max} = n_1 + n_2$. The specific smoothing process of the parking path based on the principle shown in Figure 7 is as follows:

1. The coordinate of the point G_1^{**} is calculated as $(x_{G_0^*} - n_{\max}, y_{G_0^*})$.
2. According to the planning process of one maneuver parking path in section "One-maneuver path planning" we can obtain the following parameters based on the coordinate of the point G_1^{**} and the coordinate of the point G_4 represented as $(-S_1, -W/2)$:
   2a. The coordinate of the center point O_1^{**} of the circle arc $\overset{\frown}{G_1^{**}G_2^{**}}$ is $(x_{G_0^*} - n_{\max}, y_{G_0^*} - R_{\min})$.
   2b. The coordinate of the center point O_2 of the circle arc G_3G_4 is $(-S_1, R_{\min} - W/2)$.
   2c. The angle of the circle arc $\overset{\frown}{G_1^{**}G_2^{**}}$ and the circle arc $\overset{\frown}{G_3G_4}$ are given by
   $$\theta = \arcsin\left(\frac{x_{G_0^*} - n_{\max} + S_1}{|O_1O_2|}\right) - \arccos\left(\frac{2R_{\min}}{|O_1O_2|}\right) \quad (37)$$
   2d. The coordinate of the point G_2^{**} is $(x_{G_0^*} - n_{\max} - R_{\min}\sin\theta, y_{G_0^*} - R_{\min}(1-\cos\theta))$.
   2e. The coordinate of the point G_3 is $(-S_1 + R_{\min}\sin\theta, R_{\min}(2-\cos\theta) - W/2)$.
3. The actual smoothing offset is calculated as $n_0 = n_1 + n_2\tan(\theta/2)$.
4. The coordinate of the point G_1^* is calculated as $(x_{G_1^*}, y_{G_1^*}) = (x_{G_0^*} - n_{\max} + n_0, y_{G_0^*})$.
5. The coordinates of the point G_2^* is calculated based on the coordinate of the point G_1^*, and it is represented as $(x_{G_1^*} - n_0(1+\cos\theta) - R_{\min}\sin\theta, y_{G_1^*} - R_{\min}(1-\cos\theta) - n_0\sin\theta)$.
6. The coordinates of the point G_4^* and the point G_3^* are calculated as $(-S_1 - n_0, -W/2)$, and $(-S_1 + R_{\min}\sin\theta + n_0\cos\theta, R_{\min}(2-\cos\theta) - W/2 + n_0\sin\theta)$, respectively.
7. The first half of the fixed B-spline curve given by solving the nonlinear optimization problem (36) in off-line mode is used to generate the transition curves starting with the point G_1^*, the point G_2^*, the point G_3^* and the point G_4^* based on rotation transformation and flip transformation, respectively. Specifically, the first half of the fixed B-spline curve is flipped both horizontally and vertically to generate the transition curve starting with the point G_1^*. The first half of the fixed B-spline curve is flipped horizontally and is rotated anticlockwise with the angle of the circle arc $\overset{\frown}{G_1^{**}G_2^{**}}$ to generate the transition curve starting with the point G_2^*. The first half of the fixed B-spline curve is flipped vertically and is rotated anticlockwise with the angle of the circle arc $\overset{\frown}{G_3G_4}$ to generate the transition curve starting with the point G_3^*. The first half of the fixed B-spline curve is directly used to generate the transition curve starting with the point G_4^*. Then, the circle arc with the minimum radius $R_{\min}$ and the arc angle $\theta + \phi - \pi$ are used to connect the endpoint of the transition curve starting with the point G_1^* with the endpoint of the transition curve starting with the point G_2^* smoothly and connect the endpoint of the transition curve starting with the point G_3^* with the endpoint of the transition curve starting with the point G_4^* smoothly.
8. The maximum distance from the x-axis of the coordinate system OXY to the envelope of the smooth path is conservatively estimated as
$$S_l = \left(R_{\min} + \frac{W}{2}\right)\cos\vartheta + \left(L + L_f\right)\sin\vartheta + y_{G_1^*} - R_{\min} \quad (38)$$

where $\vartheta = \min(\theta, \vartheta_{\max})$.

Longitudinal velocity planning

The task of the vehicle longitudinal velocity planning for autonomous parallel parking is to design a smooth parking velocity curve to make the vehicle start smoothly to move along the planned parking path and to make the vehicle stop smoothly at the end of the planned parking path. Therefore, the parking velocity curve can be divided into acceleration, constant velocity and deceleration segments. In this section, we adopt B-spline curve to design the acceleration and deceleration segments to implement the smooth changes of the parking velocity and acceleration under the constraints of equations (39)–(43). The design process of the acceleration segment is mainly introduced as follows, since the deceleration segment can be easily obtained by flipping the acceleration segment vertically

$$v_{start} = v_{end} = 0 \quad (39)$$

$$a_{start} = a_{end} = 0 \quad (40)$$

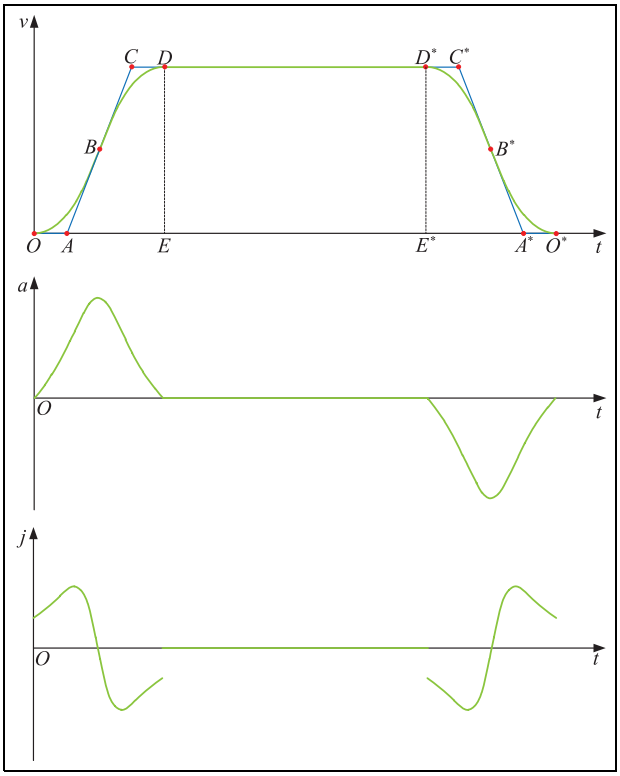

Figure 11. Parking velocity, acceleration and jerk based on B-spline curve.

$$|v| \leqslant v_{\max} \tag{41}$$

$$|a| \leqslant a_{\max} \tag{42}$$

$$|j| \leqslant j_{\max} \tag{43}$$

where v_{start} and v_{end} are the endpoint values of the parking velocity curve, respectively; a_{start} and a_{end} are the endpoint values of the parking acceleration curve, respectively; $v_{\max}$ is the maximum parking velocity; $a_{\max}$ is the maximum parking acceleration; $j_{\max}$ is the maximum parking jerk.

According to the definition of B-spline curve,[24] the parking velocity curve based on B-spline curve can be expressed as $C(u) = [t(u), v(u)]^{\mathrm{T}}$. Then, the parking acceleration curve can be described as

$$a(u) = \frac{dv}{dt} = \frac{dv}{du}\frac{du}{dt} = \frac{\dot{v}(u)}{\dot{t}(u)} \tag{44}$$

The derivative of equation (44) with respect to time, we can obtain the parking jerk curve as follows

$$j(u) = \frac{da}{dt} = \frac{da}{du}\frac{du}{dt} = \frac{\ddot{v}(u)\dot{t}(u) - \dot{v}(u)\ddot{t}(u)}{(\dot{t}(u))^3} \tag{45}$$

According to the strong convex hull property of B-spline curve,[26] we take the point O, the point D, and three collinear points A, B and C shown in Figure 11 as the control points of B-spline curve. Supposing that $|OA| = t_1$ and $|OE| = t_2$, these control points, which satisfy $|OA| = |CD|$ and $|AB| = |BC|$, are given by

$$P_x = \left[0, t_1, \frac{t_2}{2}, t_2 - t_1, t_2\right] \tag{46}$$

$$P_y = \left[0, 0, \frac{v_{\max}}{2}, v_{\max}, v_{\max}\right] \tag{47}$$

where $t_1 > 0$ and $t_2 > 0$ are unknown parameters.

According to equation (47), the constraint of equation (41) is satisfied naturally. To satisfy the constraints of equations (39) and (40), the degree of B-spline curve is set to 3 and the multiplicities of the first knot and the last knot are set to 4 to make B-spline curve pass through the first and last control points. Thus, the knot vector of the B-spline curve is given by

$$U = \{0, 0, 0, 0, 0.5, 1, 1, 1, 1\} \tag{48}$$

As shown in Figure 11, the area surrounded by the line segment OA, the line segment AB and the curve OB is equal to the area surrounded by the line segment CD, the line segment BC and the curve BD, since the control points of B-spline curve satisfy $|OA| = |CD|$ and $|AB| = |BC|$, and the three control points A, B and C are collinear. Therefore, the arc length of the planned parking path corresponding to the acceleration segment of the parking velocity curve is equal to the area of the trapezoid $AEDC$. Similarly, the arc length of the planned parking path corresponding to the deceleration segment of the parking velocity curve is equal to the area of the trapezoid $A^*E^*D^*C^*$. Furthermore, the total arc length of the planned parking path corresponding to the parking velocity curve is the sum of the area of trapezoidal $AEDC$, the area of trapezoidal $A^*E^*D^*C^*$ and the area of rectangular DD^*E^*E. Thus, the arc length of the planned parking path is taken as the path velocity correlation term to establish the relationship between the planned parking path and the parking velocity curve. To reduce the parking time by minimizing the needed time acceleration and deceleration segments, the nonlinear optimization problem (49) is obtained with two constraints of equations (42) and (43)

$$\begin{aligned} \min_{[t_1, t_2]} \quad & \frac{t_2}{2} v_{\max} \\ \text{subject to} \quad & |a| \leqslant a_{\max} \\ & |j| \leqslant j_{\max} \end{aligned} \tag{49}$$

The interior point method is used to solve the nonlinear optimization problem (49) in off-line mode to reduce the computational time, and the fixed B-spline curve is used as the acceleration and deceleration segments of the parking velocity curve.

Trajectory tracking control

Trajectory tracking control is to design a robust decoupling control strategy to make the vehicle execute the generated trajectory by simultaneously controlling the steering system, the driving system and the braking system. In this section, the trajectory tracking control problem for autonomous parallel parking of a front-

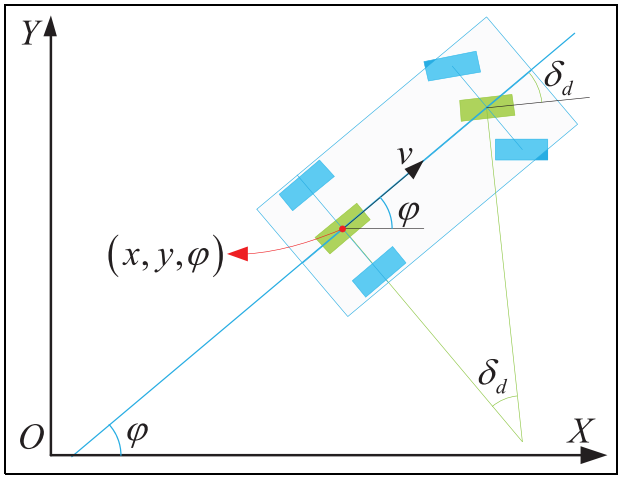

Figure 12. Kinematic model of the vehicle.

wheel steering vehicle is decoupled into the path tracking control problem and the longitudinal velocity tracking control problem by choosing the lateral displacement of the parking trajectory as the non-time reference. Specifically, a non-time reference path tracking sliding mode control strategy is developed based on Lyapunov stability theory, and a longitudinal velocity tracking PI control strategy is proposed based on smooth handoff method.

Path tracking control

The kinematic characteristics of the vehicle at low speed can be represented as the coordinate (x, y) of the reference point, which is located at the midpoint of the vehicle's rear wheel axle, and the orientation angle φ between vehicle orientation and positive direction of x-axis in counterclockwise. As shown in Figure 12, the differential equations of non-holonomic kinematics can be described as[27]

$$\begin{cases} \dot{x} = v\cos\varphi \\ \dot{y} = v\sin\varphi \\ \dot{\varphi} = \dfrac{v\tan\delta_f}{L} \end{cases} \tag{50}$$

When the vehicle moves backward, the negative of the x coordinate of the reference point is the monotone increasing function with respect to time and is selected as the non-time reference. Then, the non-time reference parking path tracking error is given by

$$\begin{cases} x_e = 0 \\ y_e = y_r(x) - y(x) \\ \varphi_e = \varphi_r(x) - \varphi(x) \end{cases} \tag{51}$$

The derivative of equation (51) with respect to the non-time reference yields

$$\begin{cases} \dfrac{dy_e}{-dx} = \dfrac{dy_r(x)}{-dx_r} - \dfrac{dy(x)}{-dx} = -\tan\varphi_r + \tan\varphi \\ \dfrac{d\varphi_e}{-dx} = \dfrac{d\varphi_r(x)}{-dx_r} - \dfrac{d\varphi(x)}{-dx} = -\dfrac{\rho_r}{\cos\varphi_r} + \dfrac{\tan\delta_d}{L\cos\varphi} \end{cases} \tag{52}$$

Define the sliding surface

$$\sigma = \kappa_0 y_e + (\tan\varphi - \tan\varphi_r) \tag{53}$$

where $\kappa_0 > 0$ is the design parameter.

According to equation (53), we can obtain the following equation when $\sigma = 0$

$$\dot{y}_e = -\kappa_0 y_e \tag{54}$$

Therefore, the state trajectory on the sliding surface can asymptotically converge to the equilibrium point of the system. Furthermore, the non-time reference path tracking sliding mode control strategy is developed to make the state trajectory converge to the sliding surface in finite time, and the following theorem is obtained.

Theorem 1. Consider the system (51) where the non-time reference path tracking sliding mode control law is defined in equation (55)

$$\delta_f = \arctan\left(L\cos^3\varphi\left(\frac{\rho_r}{\cos^3\varphi_r} + \kappa_0(\tan\varphi - \tan\varphi_r) + \kappa_1\sigma + \kappa_2\mathrm{sgn}(\sigma)\right)\right) \tag{55}$$

where $\mathrm{sgn}(\sigma)$ is the sign function. If the parameters κ_1 and κ_2 are chosen such that $\kappa_1 > 0$ and $\kappa_2 > 0$, then the equilibrium point of the closed-loop system is asymptotically stable.

Proof. Define a Lyapunov function candidate as

$$V = \frac{1}{2}\sigma^2 \tag{56}$$

Differentiating V with respect to time yields

$$\dot{V} = \sigma\dot{\sigma} \tag{57}$$

The derivative of equation (53) with respect to time yields

$$\begin{aligned} \dot{\sigma} &= \kappa_0\frac{dy_e}{-dx} + \frac{d(\tan\varphi - \tan\varphi_r)}{-dx} \\ &= \kappa_0(\tan\varphi - \tan\varphi_r) + \left(\frac{\rho_r}{\cos^3\varphi_r} - \frac{\tan\delta_f}{L\cos^3\varphi}\right) \end{aligned} \tag{58}$$

Substituting equation (58) into equation (57) yields

$$\dot{V} = \sigma\left(\kappa_0(\tan\varphi - \tan\varphi_r) + \left(\frac{\rho_r}{\cos^3\varphi_r} - \frac{\tan\delta_f}{L\cos^3\varphi}\right)\right) \tag{59}$$

Substituting equation (55) into equation (59) yields

$$\dot{V} = -\kappa_1\sigma^2 - \kappa_2\sigma\mathrm{sgn}(\sigma) = -2\kappa_1 V - \sqrt{2}\kappa_2 V^{1/2} \tag{60}$$

According to the finite time stability theorem,[28,29] the state trajectory of the closed-loop system is converged to the sliding surface $\sigma = 0$ in finite time t_r, which satisfies equation (61)

$$t_r = \frac{1}{\kappa_1}\ln\frac{2\kappa_1 V_0^{1/2} + \sqrt{2}\kappa_2}{\sqrt{2}\kappa_2} \tag{61}$$

where V_0 is initial value of the Lyapunov function candidate.

Furthermore, according to equation (54), the equilibrium point of the closed-loop system is asymptotically stable.

In the aspect of forcing the state trajectory of the closed-loop system to approach the sliding surface, equation (60) shows that the exponential rate reaching item $\kappa_1\sigma^2$ plays a dominant role when the state trajectory of the closed-loop system is far from the sliding surface, and the constant rate reaching item $\kappa_2\sigma\mathrm{sgn}(\sigma)$ plays a dominant role when the state trajectory of the closed-loop system is near from the sliding surface. Therefore, the combination of the exponential rate reaching item and the constant rate reaching item can effectively improve the dynamic response characteristics of the closed-loop system.

When the vehicle moves forward, the x coordinate of the reference point is the monotone increasing function with respect to time and is selected as the non-time reference. Similarly, the following non-time reference path tracking sliding mode control law can be deduced based on the sliding surface $\sigma = \kappa_0 y_e + (\tan\varphi_r - \tan\varphi)$

$$\delta_f = \arctan\left(L\cos^3\varphi\left(\frac{\rho_r}{\cos^3\varphi_r} + \kappa_0(\tan\varphi_r - \tan\varphi) + \kappa_1\sigma + \kappa_2\mathrm{sgn}(\sigma)\right)\right) \tag{62}$$

Longitudinal velocity tracking control

Since the driving system and the braking system are two opposing single-acting actuators, the proposed longitudinal velocity tracking PI control strategy adopts a PI error metric to complete the smooth switchover between the driving system and the braking system.[30] Then, the PI error metric based on proportional integral control method is calculated as

$$u(k+1) = u(k) + \Delta u = u(k) + K_P(e(k+1) - e(k)) + K_I e(k+1) \tag{63}$$

where K_P and K_I are the proportional and integral coefficients, respectively; $u(k+1)$ is the control input at time $k+1$; $e(k+1)$ is the velocity error at time $k+1$.

When the PI error metric is non-negative, the driving system is activated to exert a driving force proportional to the PI error metric on the vehicle; and when it is negative, the braking system is activated to exert a braking force proportional to the negative of the PI error metric on the vehicle

$$\begin{cases} T_{engine}(k+1) = K_{engine}u(k+1), T_{brake}(k+1) = 0 & u(k+1) \geqslant 0 \\ T_{engine}(k+1) = 0, T_{brake}(k+1) = K_{brake}|u(k+1)| & u(k+1) < 0 \end{cases} \tag{64}$$

where K_{engine} and K_{brake} are the gain coefficients of the driving and braking system, respectively.

Table 1. Parameters for the test vehicle.

Parameters	Notation	Value
The length of the vehicle	L_c	4.155 (m)
The width of the vehicle	W	1.645 (m)
Wheelbase	L	2.405 (m)
Front overhang	L_f	0.800 (m)
Rear overhang	L_r	0.950 (m)
The maximum front-wheel equivalent steering angle	$\delta_{\max}$	0.524 (rad)
The maximum front-wheel equivalent steering speed	$\rho_{\max}$	0.524 (rad/s)
The maximum parking acceleration	$a_{\max}$	1.000 (m/s^2)
The maximum parking jerk	$j_{\max}$	3.000 (m/s^3)

Simulation results

The parking performance of the proposed autonomous parallel parking strategy is verified based on model-in-the-loop simulation system, which is constituted of the vehicle dynamics simulation software (MSC CarSim®) and the proposed autonomous parallel parking strategy. MSC CarSim® can deliver the most accurate and efficient methods for simulating the whole vehicle dynamics to make the simulation results coincide with the real-vehicle experimental results. Parallel parking in one or more maneuvers on a flat dry asphalt road is carried out, respectively, and all parameters of the test vehicle are listed in Table 1.

Parallel parking in one maneuver

The parallel parking in one maneuver is implemented under the conditions that the length and width of the parking space are set to the minimum length and the minimum width of the parking space and the coordinate of the starting point is set to [4, 3]. The simulation results are shown in Figure 13. As shown in Figure 13(i), we can see that the reference parking path can guide the vehicle into the parking space safely. As shown in Figure 13(a), (d), (f) and (h), we can see that the proposed non-time reference path tracking sliding mode control strategy can achieve accurate and stable tracking control of the reference parking path without reorienting the steering wheel angle at the stop of vehicle. As shown in Figure 13(b), (e) and (g), we can see

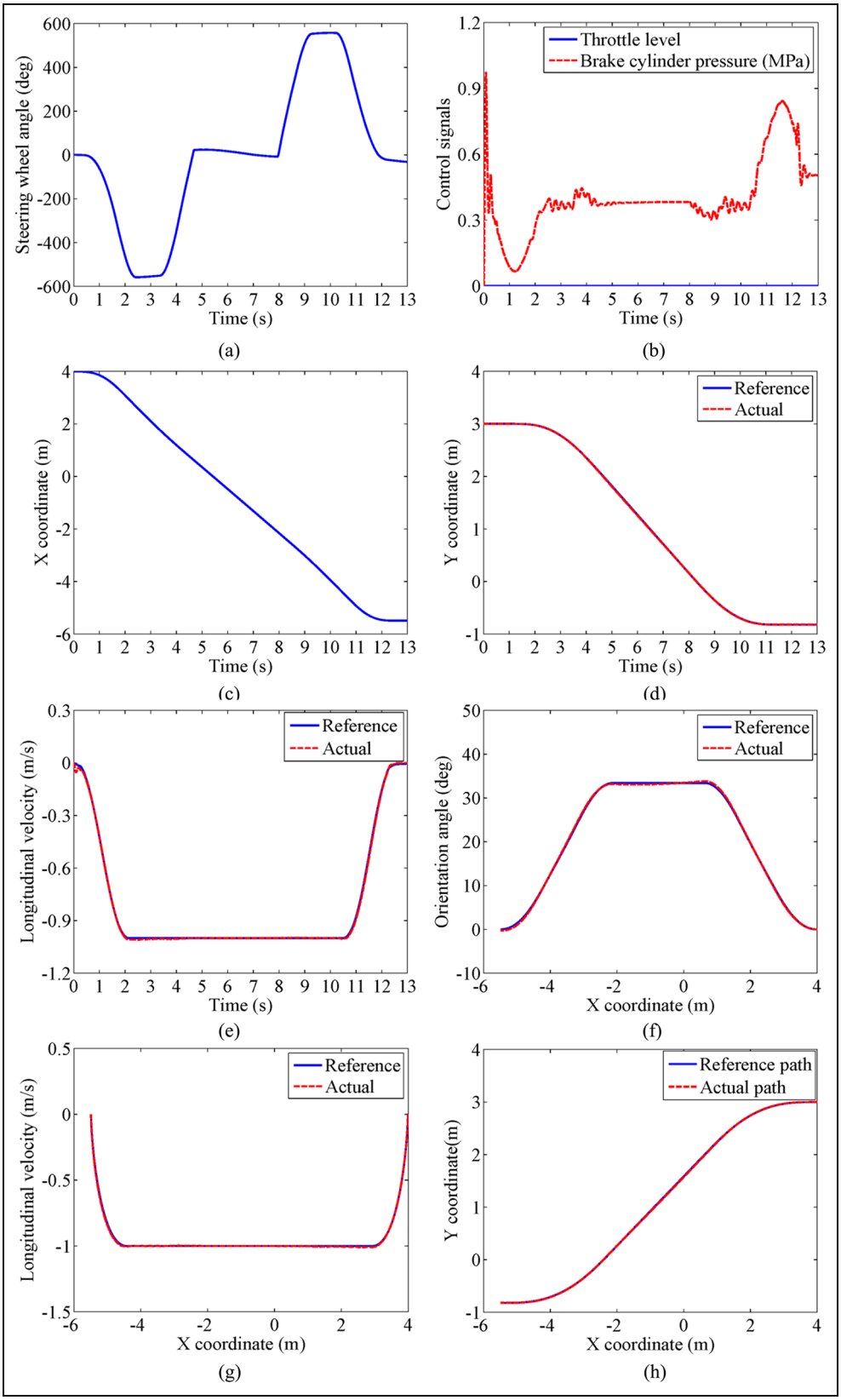

Figure 13. Continued.

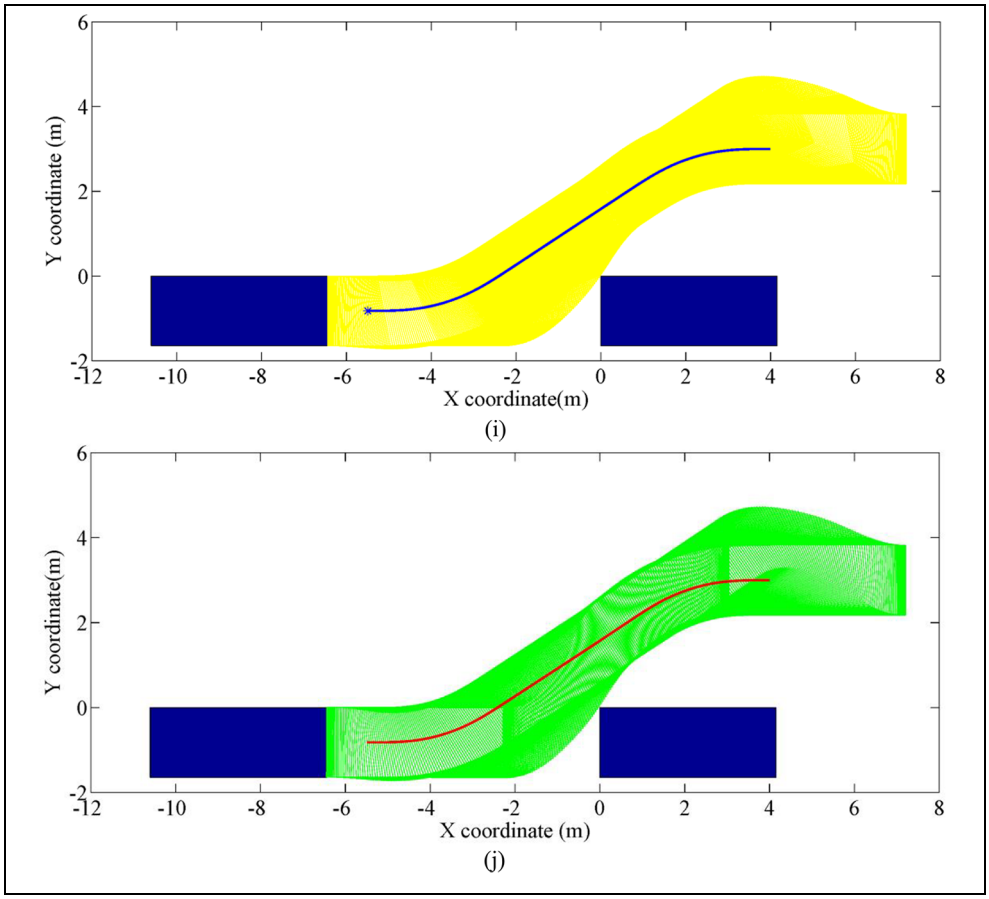

Figure 13. The simulation results of parallel parking in one maneuver: (a) steering wheel angle, (b) throttle level and brake cylinder pressure, (c) the *x* coordinate of the reference point, (d) the *y* coordinate of the reference point, (e) vehicle longitudinal velocity, (f) the orientation angle of vehicle changing with respect to the *x* coordinate of the reference point, (g) vehicle longitudinal velocity changing with respect to the *x* coordinate of the reference point, (h) the reference parking path and actual parking path, (i) the dynamic envelope of the vehicle moving along the reference parking path and (j) the dynamic envelope of the vehicle moving along the actual parking path.

that the designed longitudinal velocity tracking PI control strategy can achieve accurate and stable tracking control of the reference longitudinal velocity by smoothly switching over between the driving system and the braking system. In sum, as shown in Figure 13(j), the proposed trajectory tracking control strategy can make the vehicle execute the planned trajectory without collision by simultaneously controlling the steering system, the driving system and the braking system.

Parallel parking in multiple maneuvers

The parallel parking in multiple maneuvers is implemented under the conditions that the coordinate of the starting point is set to [4, 3], the width of the parking space is set to the minimum width of the parking space and the length of the parking space is set to 5.173 m, which is smaller than the minimum length of the parking space. The simulation results are shown in Figure 14.

As shown in Figure 14(i), we can see that the reference parking path can guide the vehicle into the parking space safely. As shown in Figure 14(a), (d), (f) and (h), we can see that the proposed non-time reference path tracking sliding mode control strategy can achieve accurate and stable tracking control of the reference parking path. First, the vehicle moves backward without reorienting the steering wheel angle at the stop of vehicle until approaching the rear obstacle. Then, the vehicle executes 3 times of forward and backward moves to enter the parking space. During forward or backward moves, the steering is done at the stop of vehicle to improve the parking space utilization. After each forward or backward move, the lateral displacement of the vehicle shown in the local enlarged drawing of Figure 14(d) is generated. As shown in Figure 14(b), (e) and (g), we can see that the designed longitudinal velocity tracking PI control strategy can achieve accurate and stable tracking control of the reference longitudinal velocity by smoothly switching over between the driving system and the braking system. In sum, as shown in Figure 14(j), the proposed trajectory tracking control

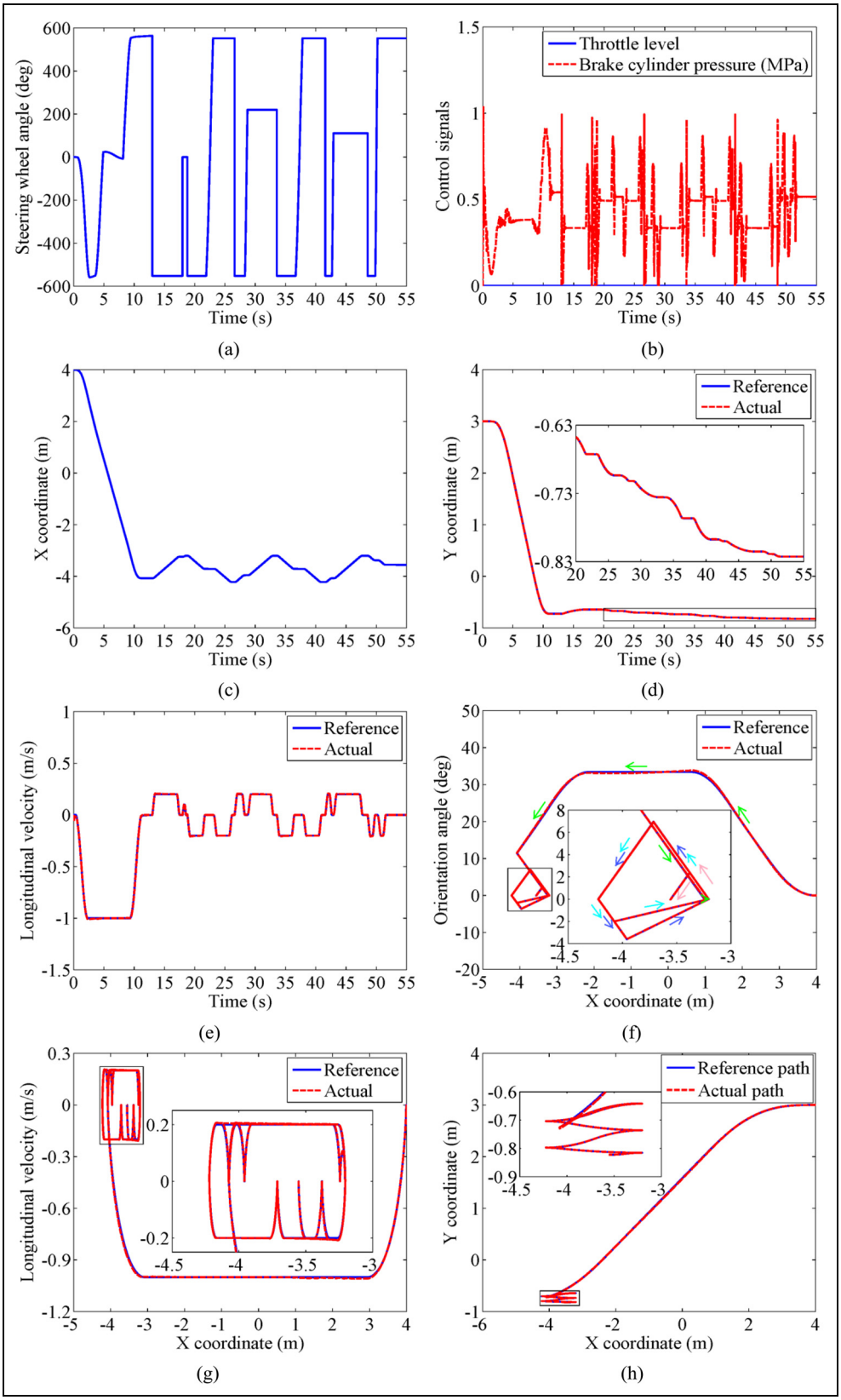

Figure 14. Continued.

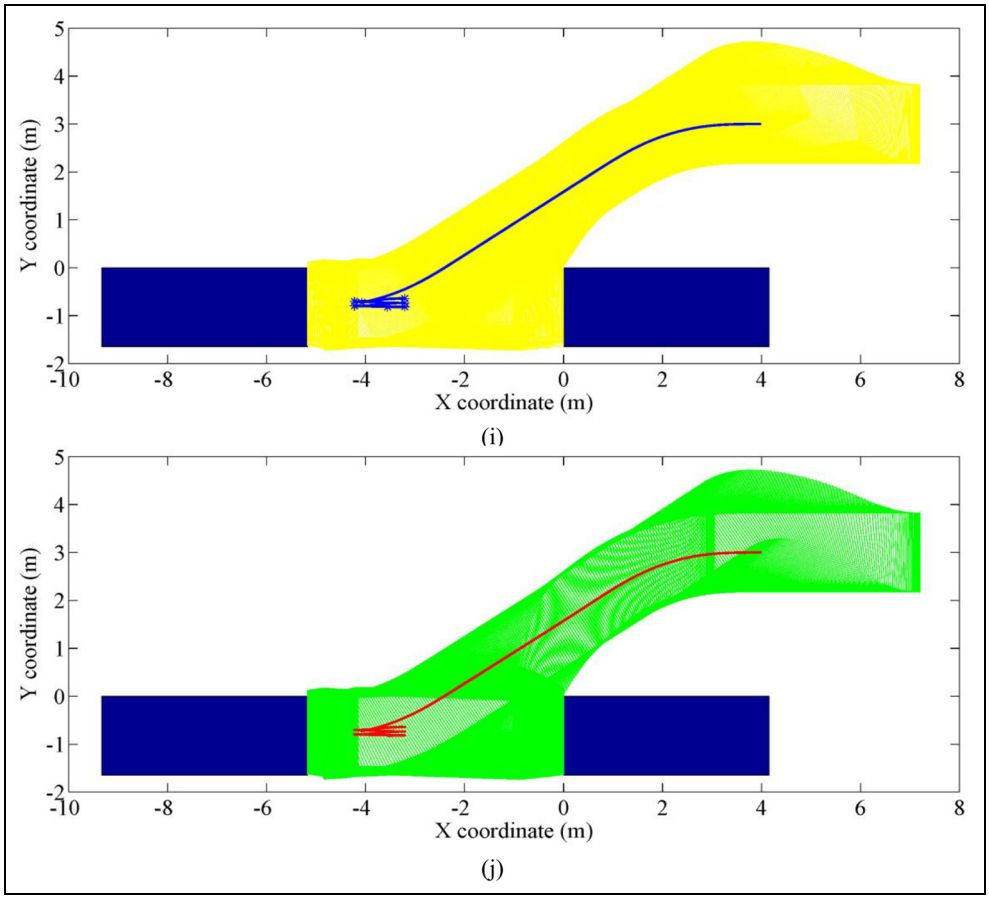

Figure 14. The simulation results of parallel parking in one maneuver: (a) steering wheel angle, (b) throttle level and brake cylinder pressure, (c) the *x* coordinate of the reference point, (d) the *y* coordinate of the reference point, (e) vehicle longitudinal velocity, (f) the orientation angle of vehicle changing with respect to the *x* coordinate of the reference point, (g) vehicle longitudinal velocity changing with respect to the *x* coordinate of the reference point, (h) the reference parking path and actual parking path, (i) the dynamic envelope of the vehicle moving along the reference parking path and (j) the dynamic envelope of the vehicle moving along the actual parking path.

strategy can make the vehicle execute the planned trajectory without collision by simultaneously controlling the steering system, the driving system and the braking system.

Conclusion

This paper has presented a novel trajectory planning method and a novel trajectory tracking control method for autonomous parallel parking of a front-wheel steering vehicle. First, a collision-free path by combining circle arcs with straight line is created to park the vehicle in one or more maneuvers, and then the path is transformed into a continuous-curvature path using B-spline curve. Second, the longitudinal velocity is created using B-spline curve. To execute the generated trajectory, a non-time reference path tracking sliding mode control strategy is deduced by Lyapunov stability theory, and a longitudinal velocity tracking PI control strategy is proposed based on smooth handoff method. Finally, the simulation is implemented to validate the parking performance, and the simulation results show that it can guarantee that the vehicle parks in the narrow parking space safely and accurately.

Declaration of conflicting interests

The author(s) declared no potential conflicts of interest with respect to the research, authorship and/or publication of this article.

Funding

The author(s) received no financial support for the research, authorship and/or publication of this article.

ORCID iD

Jiaxu Zhang https://orcid.org/0000-0001-6159-1965

References

1. He DF, He WT and Song XL. Efficient predictive cruise control of autonomous vehicles with improving ride comfort and safety. *Meas Control* 2020; 53(1–2): 18–28.

2. Zhang RH, He ZC, Wang HW, et al. Study on self-tuning tyre friction control for developing main-servo loop integrated chassis control system. *IEEE Access* 2017; 5: 6649–6660.
3. Zhang JX and Li J. Adaptive backstepping sliding mode control for wheel slip tracking of vehicle with uncertainty observer. *Meas Control* 2018; 51(9–10): 396–405.
4. Zhao XL, Zhang Y and Zhao BX. Robust path planning for avoiding obstacles using time-environment dynamic map. *Meas Control* 2020; 53(1–2): 214–221.
5. Moran A and Nagai M. Autonomous parking of vehicles with intelligent fuzzy-neural networks. *JSAE Rev* 1995; 16(2): 270–275.
6. Zhao YN and Collins EG. Robust automatic parallel parking in tight spaces via fuzzy logic. *Robot Auton Syst* 2005; 51: 111–127.
7. Ryu Y, Oh S and Kim S. Robust automatic parking without odometry using an evolutionary fuzzy logic controller. *Int J Control Autom* 2008; 6(3): 434–443.
8. Lee CK, Lin CL and Shiu BM. Autonomous vehicle parking using hybrid artificial intelligent approach. *J Intell Robot Syst* 2009; 56(3): 319–343.
9. Demirli K and Khoshnejad M. Autonomous parallel parking of a car-like mobile robot by a neuro-fuzzy sensor-based controller. *Fuzzy Set Syst* 2009; 160: 2876–2891.
10. Zheng GQ, Zhao L and Li JS. Optimization of an intelligent controller for parallel autonomous parking. *TELKOMNIKA Indones J Electr Eng* 2013; 11(2): 1069–1075.
11. Wang Y and Zhu XX. Hybrid fuzzy logic controller for optimized autonomous parking. In: *Proceedings of the 2013 American control conference*, Washington, DC, 17–19 June 2013.
12. Liu W, Li ZH, Li L, et al. Parking like a human: a direct trajectory planning solution. *IEEE T Intell Transp* 2017; 18(12): 3388–3397.
13. Xu Y, Lu ZF, Shan X, et al. Study on automatic parking method based on the sliding mode variable structure and fuzzy logical control. *Symmetry* 2018; 10(10): 523–535.
14. Xu J, Xie M and Lu JZ. Duplex motion planning strategy for automatic manoeuvre of vehicle in complex environment. In: *Proceedings of the 2001 IEEE intelligent transportation systems conference*, Oakland, CA, 25–29 August 2001, pp. 292–297. New York: IEEE.
15. Zhdanov AA, Klimov DM, Korolev VV, et al. Modeling parallel parking a car. *J Comput Sys Sc Int* 2008; 47(6): 907–917.
16. Kim D, Chung W and Park S. Practical motion planning for car-parking control in narrow environment. *IET Control Theory A* 2010; 4(1): 129–139.
17. Zhao L, Zheng GQ and Li JS. Automatic parking path optimization based on Bezier curve fitting. In: *Proceedings of the 2012 IEEE international conference on automation and logistics*, Zhengzhou, China, 15–17 August 2012.
18. Chand A, Kawanishi M and Narikiyo T. Application of sigmoidal Gompertz curves in reverse parallel parking for autonomous vehicles. *Int J Adv Robot Syst* 2015; 12(9): 1–11.
19. Vorobieva H, Glaser S, Minoiu-Enache N, et al. Automatic parallel parking in tiny spots: path planning and control. *IEEE T Intell Transp* 2015; 16(1): 396–410.
20. Jang C, Kim C, Lee S, et al. Re-plannable automated parking system with a standalone around view monitor for narrow parking lots. *IEEE T Intell Transp* 2020; 21(2): 777–790.
21. Zips P, Bock M and Kugi A. Optimisation based path planning for car parking in narrow environments. *Robot Auton Syst* 2016; 79: 1–11.
22. Chai R, Tsourdos A, Savvaris A, et al. Two-stage trajectory optimization for autonomous ground vehicles parking maneuver. *IEEE T Ind Inform* 2018; 15(7): 3899–3909.
23. Yang Y, Zhang L, Qu X, et al. Smooth path planning for autonomous parking system. In: *Proceedings of the 2017 IEEE intelligent vehicles symposium*, Redondo Beach, CA, 11–14 June 2017.
24. Hearn D and Pauline Baker M. *Computer graphics with openGL*. 3rd ed. Englewood, CO: Prentice Hall, 2003, pp. 100–102.
25. Kim SJ, Koh K, Lustig M, et al. An interior-point method for large-scale L1-regularized least squares. *IEEE J Sel Top Signa* 2007; 1(4): 606–617.
26. Elbanhawi M, Simic M and Jazar RN. Continuous path smoothing for car-like robots using B-spline curves. *J Intell Robot Syst* 2015; 80(1): 23–56.
27. Zhao J, Chen ZC, Zhu B, et al. Precise active brake-pressure control for a novel electro-booster brake system. *IEEE T Ind Electron* 2020; 67(6): 4774–4784.
28. Nadafi R, Kabganian M, Kamali A, et al. Super-twisting sliding mode control design based on Lyapunov criteria for attitude tracking control and vibration suppression of a flexible spacecraft. *Meas Control* 2019; 52(7–8): 814–831.
29. Yu SD, Ma JY, Wu HT, et al. Robust precision motion control of piezoelectric actuators using fast nonsingular terminal sliding mode with time delay estimation. *Meas Control* 2019; 52(1–2): 11–19.
30. Thrun S, Montemerlo M, Dahlkamp H, et al. Stanley: the robot that won the DARPA grand challenge. *J Field Robot* 2006; 23: 661–692.